JOURNAL OF COLLOID AND INTERFACE SCIENCE **202,** 124–138 (1998)
ARTICLE NO. CS985416

Compound Complex Formation in Phospholipid Membranes Induced by a Nonionic Surfactant of the Oligo(ethylene oxide)–Alkyl Ether Type: A Comparative DSC and FTIR Study

B. Mädler, H. Binder,[1] and G. Klose

Institute of Experimental Physics I, University of Leipzig, Physics of Biomembranes, Linnéstrasse 5, D-04103 Leipzig, Germany

Received September 22, 1997; accepted January 6, 1998

The phase behavior of pseudobinary mixtures DMPC/$C_{12}E_4$ at high water excess was studied between 0 and 50°C as a function of the surfactant mole fraction x using DSC and FTIR. The phase transitions of each component could be followed separately by FTIR spectroscopy mixing acyl-chain-deuterated DMPC-d_{54} and alkyl-chain-protonated $C_{12}E_4$. Changes of the corresponding methylene stretching band frequencies yield the solidus and liquidus lines in the temperature–composition phase diagram. Two eutectics appear at $x \approx 0.55$ and $x \approx 0.85$. In the concentration range in between these values, the existence of a gel compound complex of about 1:2 lipid:surfactant composition was established. A peritectic point was suggested at low surfactant concentration between the rippled, gel, and liquid crystalline states of the lipid-rich bilayers on the basis of the Gibbs phase rule. A micellar transition (cloud point) precedes the formation of lamellar aggregates as the surfactant rich mixtures are heated. The phase transformations are discussed in terms of fluidity and hydration of the molecules on the basis of spectral data obtained from selected infrared absorption bands of the lipid and of the surfactant. The phase behavior of $C_{12}E_4$/DMPC was compared with literature data of related systems with respect to the chain melting transition, membrane solubilization, and complex formation.

Key Words: **thermotropic phase behavior; eutectic mixture; lamellar and micellar phases; hydration; molecular order.**

INTRODUCTION

In an aqueous environment phospholipids assemble spontaneously into bilayers, which represent the basic structural unit of biological membranes. Studies of how bilayer structure and thermodynamic properties vary as bilayer composition is varied are important tools for improving our knowledge about membrane stability and function. Several strategies can be used to alter the balance of interactions within the bilayer. One approach, suggested by the amphiphilic character of the lipid molecules, is to add surfactants to the lipid matrix and thus to vary the hydrophilic/hydrophobic balance in a definite way. The incorporation of nonionic surfactants of the oligo(ethylene oxide)–alkyl ether type (C_mE_n) into phospholipid bilayers is known to modulate membrane properties such as hydration (1–3), structural and dynamic properties of the membrane/water interface (4–7), partition of the surfactant between the lipid/surfactant mixed membrane and water (8), the morphology of the aggregates formed (9–11), the type of phase transitions (12–14), and the repulsive forces between the membranes (15). The lateral arrangement of membrane components such as mixing properties, cluster formation, and the solubilization of lamellar membrane structures to structures with lower symmetry and higher curvatures are of fundamental interest.

In a manner similar to that found for fatty acids and alkanols and their derivatives (16, 17), C_mE_n surfactants usually destabilize the bilayer and cause their solubilization into mixed micelles after reaching a critical fraction in the lipid membrane. The pure surfactants dissolved in water can provide a variety of lamellar and nonlamellar phases in dependence on the water concentration and temperature (18–20, 24, 25). Hence, reversible transformations between lamellar and micellar phases can be controlled by external parameters. Therefore nonionic surfactants of the C_mE_n type have been widely used for the purpose of isolation and purification of membrane proteins and for membrane reconstitution (21, 22). One prerequisite for this application is the detailed knowledge of the phase behavior of the aqueous pseudobinary lipid/surfactant mixtures in dependence on temperature and composition.

Under certain conditions selected surfactants such as short-chain n-alkanols (17) and C_mE_n with shorter ethoxy chains can stabilize lipid membranes. For example, $C_{12}E_n$ with $n < 3$ are found to fit into lipid bilayers without a disturbing effect (7). Recent calorimetric studies revealed the existence of surfactant/lipid complexes in the gel state of mixed $C_{10}E_7$/PC (9, 10) and $C_{12}E_4$/DPPC (12) bilayers (PC, phosphatidylcholine; DPPC, dipalmitoyl-PC). Com-

[1] To whom correspondence should be addressed. E-mail: binder@rz.uni-leipzig.de.

0021-9797/98 $25.00

plex formation was suggested to be caused by an optimal sterical matching of the lipid and the surfactant.

The purposes of the present paper are the following: First, we report the phase transitions of a selected lipid/surfactant mixture in dependence on temperature and surfactant mole fraction. In particular, the possibility to trigger lamellar–micellar transformations by temperature variation is of practical interest. Second, we characterize the conditions under which the surfactant–lipid interactions stabilize the bilayers in order to obtain further insight into the origin of this somewhat unusual phenomenon. Third, we chose a combination of the synthetic phospholipid L-α-1,2-dimyristoyl-*sn*-glycero-3-phosphatidylcholine (DMPC) with the nonionic surfactant tetraethylene oxide–monododecyl ether ($C_{12}E_4$) because both components are expected to match in their hydrophobic and hydrophilic parts as well. In this sense the present study continues previous investigations on $C_{10}E_7$/PC (9, 10) and $C_{12}E_4$/DPPC (12) mixtures in order to generalize the phase behavior and complex formation in lipid/surfactant systems.

The thermotropic phase behavior of the DMPC/$C_{12}E_4$ mixture was studied by varying the composition from pure lipid to pure surfactant in the temperature range $0°C < T < 50°C$ at high water excess ($200 < R_w < 50.000$; R_w is the molar ratio water to amphiphile) using highly sensitive differential scanning calorimetry (DSC) and Fourier transformed infrared spectroscopy (FTIR). The former method yields the basic thermodynamic information about main transition temperatures, transition widths, and enthalpies. Vibrational spectroscopy provides macroscopic as well as microscopic information on structural properties of molecular assemblies by means of semiempirical parameters. Discrete frequency ranges in the spectra can be assigned to the lipid and surfactant component and, moreover, to different parts of the molecules (e.g., PC headgroup, methylene chains, ethoxy chains). Therefore information about local molecular properties is available. We will show that both methods yield complementary results which allow detailed characterization of lipid/surfactant mixtures.

MATERIALS AND METHODS

Materials and Sample Preparation

DMPC and acyl-chain-perdeuterated DMPC-d_{54} were purchased from Avanti Polar Lipids Inc., Alabaster, Alabama, and used without further purification after thin-layer chromatography and DSC check. The nonionic surfactant $C_{12}E_4$ was provided by Nikko Chemicals, Tokyo. Its purity was guaranteed by DSC and melt point measurements. The deuteration of the ethoxy (EO) chains in $C_{12}E_4$-d_{16} was realized by etherification (63) of perdeuterated tetra-(oxyethylene) glycol (synthesized as described in Ref. (64)) and $CH_3(CH_2)_{11}Br$. The deuterated alkyl chain analog, $C_{12}E_4$-d_{25}, was synthesized by etherification of tetraethylene glycol and $CD_3(CD_2)_{11}Br$ (Euriso-top, France).

The samples were prepared by dissolving the components at definite molar fractions of the surfactant x in three times distilled and carbon dioxide degassed water. The mixtures with deuterium-labeled DMPC-d_{54} were dispersed in 99.98% ^2H-isotopic-depleted water obtained from Merck, Germany. The mixing of the lipid, surfactant, and water was completed via vortexing in the liquid crystalline phase without using any organic solvent or sonification.

Samples with water to amphiphile (lipid plus surfactant) molar ratios of R_w between 50 and 50,000 were prepared for DSC measurements. The FTIR measurements were exclusively performed at $R_W = 200$. It was proven by DSC measurements that the water concentration has no effect on the phase transition temperatures at $R_w > 100$. The water–membrane partition coefficient of $C_{12}E_4$ is on the order of 10^6 (8). We estimated that at $R_w > 100$ more than 97% of the total amount of surfactant is situated within the aggregates. Consequently, the aqueous surfactant/lipid mixture represents a pseudobinary system to a good approximation.

Differential Scanning Calorimetry

DSC measurements of diluted samples were performed with the highly sensitive adiabatic twin calorimeter DASM-4 (Privalov calorimeter) and a Perkin–Elmer DSC-7 using heating and cooling rates between 0.1 and 1 K/min.

The onset and completion temperatures of the phase transitions were determined at the points of a baseline departure of 3% from the maximum transition intensity (30). For sharp transitions and eutectic peaks we considered the temperatures at the peak maximum. The transition temperatures were extrapolated to the limiting scan rate of 0 K/min. The transition enthalpies, ΔH_{cal}, were obtained by integrating the thermograms over the whole phase transition range.

Fourier Transform Infrared Spectroscopy

Infrared spectra with a resolution of 2 cm^{-1} were measured in the transmission mode using a Bio-Rad FTS-60a Fourier transform infrared spectrometer. The samples were filled into a thermostated liquid cell equipped with ZnSe windows and a 25-μm spacer in between. Absorbance spectra of the sample were calculated using the water spectrum as background. Typically, 256 scans were accumulated.

The samples were investigated by means of increasing as well as decreasing temperature. The temperature was varied in steps of 0.5 or 1 K and regulated with an accuracy of ± 0.1 K using an external PT-100 thermosensor fixed directly to the cell. Prior to the measurement the sample was allowed to equilibrate for at least 15 min after reaching the prescribed temperature in each step. No significant hysteresis effects were observed by this procedure, which corresponds to average heating/cooling rates of 0.04–0.02 K/min.

TABLE 1

Assignments of Selected Absorption Bands of DMPC-d_{54} and $C_{12}E_4$, the Corresponding Wavenumbers at Maximum Position, and Their Increments at Various Phase Transitions

Component	Vibration	Symbol	Fraction x	Position[a] (cm^{-1})	Increment/cm^{-1}				
					Gel[b]–L_α	$L_{\beta'}$–$P_{\beta'}$	Gel[b]–L_1	L_1–(L_1 + W)	(W + L_1)–L_α
DMPC-d_{54}	CD_2 symmetric stretching	$\nu_s(CD_2)$	0	2089.5	+4	0	—	—	—
			0.93	2090.5	—	—	+5	−2	+3
	C=O stretching	ν(C=O)	0	1736	−1.5	−0.5	—	—	—
			0.93	1730	—	—	−2	0	+5
	PO_2^- antisymmetric stretching	$\nu(PO_2^-)$	0	1230	0	0	—	—	—
			0.93	1228	—	—	−5	0	0
$C_{12}E_4$	CH_2 symmetric stretching	$\nu_s(CH_2)$	0.3	2852	+2.5	—	—	—	—
			1	2853	—	—	+2	−0.5	+1
	CH_2 wagging (ethoxy groups)	$\gamma_w(CH_2)_{EO}$	0.3	1349	0	—	—	—	—
			1	1350	—	—	0	+0.5	+0.5

Note. The first row corresponds to low and the second to high surfactant concentration, x. Wavenumbers are given with an accuracy of ±0.5 cm^{-1}. Pronounced relative wavenumber shifts are underlined.

[a] Wavenumber at maximum intensity in the gel phase (T = 5°C): pure DMPC-d_{54} (x = 0) or $C_{12}E_4$ at x = 0.93.

[b] Without differentiation between L_β, L_β', or P_β'.

Several vibrational modes originating from the hydrocarbon chains and from the polar parts of the lipid and the surfactant were analyzed in order to characterize the $C_{12}E_4$/DMPC-d_{54} pseudobinary mixture on a molecular level by means of semiempirical spectral parameters (Table I). The absorption bands were evaluated in terms of the center of gravity (COG) and width. These parameters are sensitive to shifts of the band maximum as well as to changes of the bandshape, and consequently they are well suited to detect subtle spectral changes induced by conversions of the physical state of the sample.

To characterize the surfactant alkyl chains by means of the $\nu_s(CH_2)$ mode, one has to consider that the CH_2 units in the ethoxy chains also contribute to the $\nu_s(CH_2)$ band. Figure 1a shows the CH stretching region of the surfactants $C_{12}E_4$-d_{16} and $C_{12}E_4$-d_{25} with selectively deuterated ethoxy and alkyl chains, respectively. The $\nu_s(CH_2)$ band of the ethoxy methylenes is filtered out in the spectrum of the latter species. The ethoxy methylenes absorb at distinct higher wavenumbers than the alkyl methylenes. Therefore the $\nu_s(CH_2)$ band of the completely protonated surfactant is only weakly distorted by the ethoxy methylenes except for a systematic shift of the COG of about 1 cm^{-1} and a distinct broadening (cf. Fig. 1a). To minimize this latter interference we calculate the width at 75% of the maximum height instead of the usual half maximum height.

The absorption band at about 1350 cm^{-1}, evident in the spectrum of completely protonated $C_{12}E_4$ and of $C_{12}E_4$-d_{25}, disappears for $C_{12}E_4$-d_{16} and thus is assigned to the deformation mode of the ethoxy methylenes caused mainly by their wagging vibration (31–33) (cf. Fig. 1b). The spectral overlap between the antisymmetric phosphate stretching vibration, $\nu_{as}(PO_2^-)$, and the CH_2 twisting mode of the ethoxy methylenes located at about 1250 cm^{-1} causes a systematic shift of the apparent COG($\nu_{as}(PO_2^-)$) toward higher wavenumbers in the DMPC-d_{54}/$C_{12}E_4$ binary mixture with increasing x. To eliminate this effect we subtract the x-weighted spectrum of the pure surfactant from the spectral range of the phosphate band in the spectrum of the mixture.

Infrared spectroscopy can be used to study the phase behavior directly. If in the pseudobinary system the lipid component with perdeuterated acyl chains is mixed with the surfactant component having protonated alkyl chains, then the phase state of each component may be monitored separately in a single experiment because the C–D stretching modes are well separated from the respective C–H modes by a spectral shift of about 800 cm^{-1} to lower wavenumbers (cf. Table I).

In the two-phase coexistence range a spectroscopic parameter, y_c, originating from component c = L or D of the binary mixture (L . . . lipid, D . . . surfactant; for example the center of gravity of the symmetric methylene stretching bands of $C_{12}E_4$) represents the weighted arithmetic mean of its value in the pure phases y_c^{p1} and y_c^{p2}, i.e.,

$$y_c = \frac{x_c^{p1} \cdot g_1 \cdot y_c^{p1} + x_c^{p2} \cdot g_2 \cdot y_c^{p2}}{x_c^{p1} \cdot g_1 + x_c^{p2} \cdot g_2}. \qquad [1]$$

The weighting factors g_1 and g_2 take into account that the spectroscopic responses in both phases can be different for the same amount of matter. In the case of absorption measurements they are given by the extinction coefficients of the corresponding bands in both phases, i.e., $g_1 = \epsilon_1$ and g_2

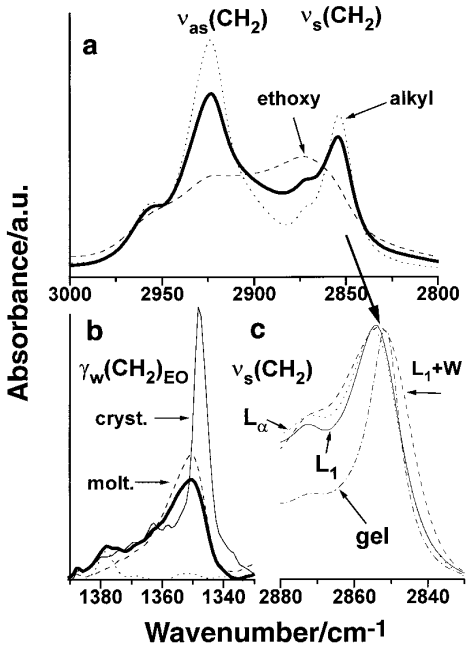

FIG. 1. IR absorbance spectra in the range of the CH_2 stretching modes (a,c) and of the ethoxy CH_2 wagging vibration (b) of fully hydrated $C_{12}E_4$. (a) $C_{12}E_4$ fully protonated (solid line) and deuterated alkyl ($C_{12}E_4$-d_{25}; dashed line) and ethoxy ($C_{12}E_4$-d_{16}, dotted line) chains. (b) $\gamma_w(CH_2)_{EO}$ band of $C_{12}E_4$ with molten ethoxy chains having the same designations as in (a) and of dry $C_{16}E_4$ with crystalline ethoxy chains (thin solid line); T = 25°C. (c) $\nu_s(CH_2)$ band of $C_{12}E_4$ in different phases: L_1 (x = 1, T = 5°C, full line); L_1 + W (x = 1, 20°C, dashed); L_α (x = 1, 24°C, dotted); gel (x = 0.6, T = 5°C, dash–dot). Spectra are normalized for comparison of peak position and bandwidth.

$= \epsilon_2$. We estimated the ratio g_1/g_2 from the corresponding integral band intensities. Rearrangement of Eq. [1] yields the fraction of each component being in phases p2,

$$x_c^{p2} = \frac{y_c - y_c^{p1}}{y_c \cdot (1 - g_1/g_2) + y_c^{p2} \cdot \dfrac{g_1}{g_2} - y_c^{p1}}, \qquad [2]$$

and p1, $x_c^{p1} = 1 - x_c^{p2}$ (e.g., p1 = L_β and p2 = L_α). The values of y_c corresponding to the pure phases, y_c^{p1} and y_c^{p2}, are found by extrapolation of the courses of y_c from the single phase ranges into the region of coexistence (see, e.g., Fig. 4). In the coexistence range the mole fraction of the surfactant existing in phase p = p1, p2 is (34)

$$x^p = \frac{x_D^p \cdot x}{x_D^p \cdot x + x_L^p \cdot (1 - x)}, \qquad [3]$$

where x denotes the mole fraction of the surfactant in the sample. Note that for gel/liquid-crystalline coexistence (i.e., p = gel, L_α), the solidus and liquidus lines in the T–x phase diagram are given by the temperature dependencies of x^{gel} and $x^{L\alpha}$, respectively.

For comparison with DSC-transition temperatures of the protonated species, it should be taken into account that deuteration shifts the transition temperatures of lipids. For DMPC-d_{54} a decrease of the gel to liquid crystalline main transition temperature between 3 and 5 K was observed compared to aqueous dispersions of protonated DMPC (27, 28). We extrapolated the phase transition temperature T_D of DMPC-d_{54}/$C_{12}E_4$ dispersions at molar fraction x to that of a fully protonated mixture (T_H) by applying the linear function

$$T_H = T_D + 3 \cdot (1 - x). \qquad [4]$$

RESULTS

DSC

Some representative DSC plots of the pseudobinary DMPC/$C_{12}E_4$ mixture at different compositions are shown in Fig. 2. A distinct decrease of the gel to liquid crystalline phase transition (main transition) temperature of the lipid is observed by incorporating $C_{12}E_4$ into the DMPC bilayer membranes. Beginning from the pure DMPC/water dispersion (x = 0) and increasing the surfactant concentration, the pretransition at 13°C vanishes completely between x = 0.08 and 0.1 and the width of the main transition increases contin-

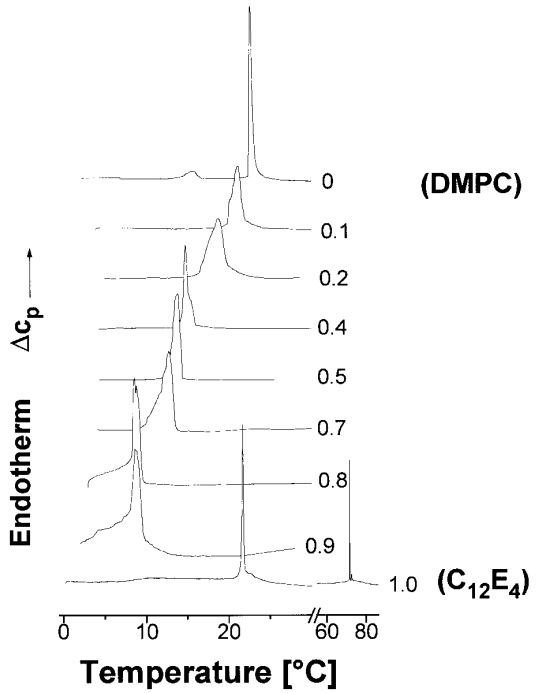

FIG. 2. Representative DSC thermograms of aqueous dispersions of mixtures of DMPC-d_{54} and $C_{12}E_4$ at a scan rate of 0.5 K/min. The figure on each thermogram indicates the molar fraction x. Cooling scans (not drawn) qualitatively showed the same behavior.

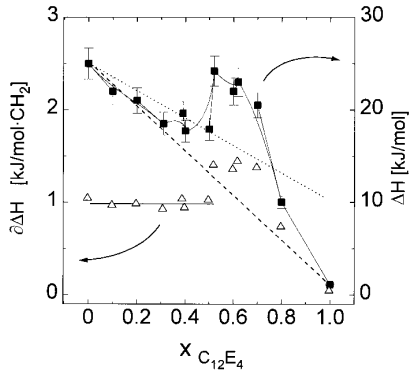

FIG. 3. Dependence of the molar transition enthalpy change ΔH (solid squares, right scale) and the incremental transition enthalpy $\delta\Delta H$ (open triangles, left scale) obtained from heating scans as a function of molar fraction x. The dashed line depicts calculated ΔH^{ideal} for an assumed ideal mixing of DMPC and $C_{12}E_4$. The dotted line fits the molar transition enthalpy assuming a constant contribution of each CH_2 group of $\delta\Delta H = 1.1$ kJ/(mol·CH_2). See text for details.

uously. Between $x = 0.4$ and $x = 0.5$, however, the transition peak becomes very narrow ($\Delta T_{1/2} = 2K$) and up to $x = 0.65$ the shape and position of this peak remain nearly constant at 13°C. Further increase of the surfactant concentration ($0.7 > x > 0.65$) leads to a downward shift and broadening of the DSC peaks, which implies the superposition of several processes. The position of the peak does not change at $0.95 > x > 0.7$ whereas a steadily increasing baseline shift at its low temperature flank indicates a non-first-order transition preceding the first-order transition at 8.5°C. Above $x = 0.95$ only one sharp peak appears. Its position shifts from 8.5°C up to 21°C at $x = 1$. Water dispersions of pure $C_{12}E_4$ ($x = 1$) show an additional narrow transition at 71.3°C.

Information about the transition type and about the miscibility of the components can be obtained from the molar transition enthalpy of the phase transformation (30)

$$\Delta H = \frac{\Delta H_{\text{cal}}}{n_{\text{DMPC}} + n_{C_{12}E_4}}, \qquad [5]$$

which is drawn in Fig. 3 (solid squares) as a function of x. ΔH_{cal} represents the transition enthalpy measured calorimetrically. n_{DMPC} and $n_{C_{12}E_4}$ denote the moles of lipid and surfactant in the sample. The error bars consider composition uncertainties and calibration errors occurring in the diluted systems. The dashed line in Fig. 3 was calculated according to

$$\Delta H^{\text{ideal}} = (1 - x)\cdot\Delta H_{\text{DMPC}} + x\cdot\Delta H_{C_{12}E_4}. \qquad [6]$$

It assumes ideal mixing of the components. $\Delta H_{\text{DMPC}} = 25$ kJ/mol and $\Delta H_{C_{12}E_4} = 1$ kJ/mol are the experimental molar transition enthalpies of the pure lipid/water and surfactant/water dispersions, respectively. The dotted line refers to ideal mixing of both components assuming a constant contribution of each CH_2 group of $\delta\Delta H = 1.1$ kJ/(mol·CH_2). This characteristic value corresponds to the hydrocarbon chain melting in lamellar aggregates (e.g., the gel to liquid crystalline transition (35)) and predicts a molar transition enthalpy of about 12 kJ/mol for the $C_{12}E_4$/water dispersion ($x = 1$). However, the measured value amounts only to 1 kJ/mol because it originates from the transition between two fluid states, namely the micellar and the lamellar liquid crystalline phases (24, 25).

The different types of phase transitions appearing at low and high surfactant contents become more obvious if one plots the measured incremental transition enthalpy, $\delta\Delta H$ (i.e., ΔH_{cal} per methylene unit of the mixture) in dependence on x (Fig. 3, open triangles). $\delta\Delta H$ adopts constant values about 1 kJ/(mol·CH_2) at surfactant mol fractions $x < 0.5$. Note that in the pseudobinary DPPC/$C_{12}E_4$ system studied recently (12) the incremental enthalpy increases drastically under similar conditions. In the concentration range where only one relatively sharp transition peak was observed ($0.5 < x < 0.7$) $\delta\Delta H$ amounts to 1.5 kJ/(mol·CH_2). Above $x = 0.7$, it decreases continuously to $\delta\Delta H < 0.1$ kJ/(mol·CH_2) at $x = 1$.

FTIR Measurements

Upon heating, the infrared spectra of aqueous $C_{12}E_4$/DMPC-d_{54} mixtures reveal typical shifts of the centers of gravity of the CH_2 and CD_2 stretching bands, indicating phase transformations within the sample (Fig. 4). The COG curves, however, behave quite differently for concentrations $x < 0.7$ and $x > 0.7$. In the former systems the hydrocarbon melting transition between the lamellar gel and liquid-crystalline phases is indicated by the marked increase of the COGs of the methylene stretching bands. At $x > 0.7$, micelles can coexist with mixed bilayers, leading to ranges of alternating slopes of the COG curves which can be attributed to different phase ranges (see below). Figure 5 compares the onset and completion temperatures of the DSC peaks (open circles) with those of the wavenumber shifts measured by FTIR (open triangles). The results of both methods agree within the limits of experimental error. Owing to different spectral features, the gel–L_α and the lamellar–micellar transitions will be analyzed separately.

Gel–L_α Phase Transition in Mixed Membranes at $x < 0.7$

Hydrocarbon chains. At surfactant mole fractions $x < 0.7$, the lipid and $C_{12}E_4$ assemble into mixed bilayers in the whole temperature range investigated. Upon heating, the membranes undergo the transition from the rigid gel ($L_{\beta'}$, $P_{\beta'}$, L_β, L_k; see discussion) into the liquid-crystalline (L_α) phase. The transition temperature decreases with increasing surfactant content in accordance with the DSC thermograms (cf. Fig. 4). The solidus and liquidus lines for gel–L_α coexistence are calculated

using Eqs. [2] and [3] with $y_D = COG(\nu_s(CH_2))$ and $y_L = COG(\nu_s(CD_2))$ measured at $x = 0.3$ and 0.6 (Fig. 5, solid squares). This agrees well with the x dependencies of the onset and completion temperatures of the melting transition derived from the DSC scans. The slightly smaller transition interval of the FTIR-data at $x = 0.3$ might be caused by the much slower average scan rate used in the infrared measurements. Both methods, however, give evidence of an essential narrowing of the coexistence range at intermediate surfactant mole fractions $0.5 < x < 0.7$.

The first derivative of the COG curves suggests a slightly restrained melting of the lipid acyl chains with respect to the dodecyl chains of the surfactant (cf. Fig. 6). This relative shift remains evident also in the cooling scan where, in reverse order, the myristoyl chains freeze first. Obviously,

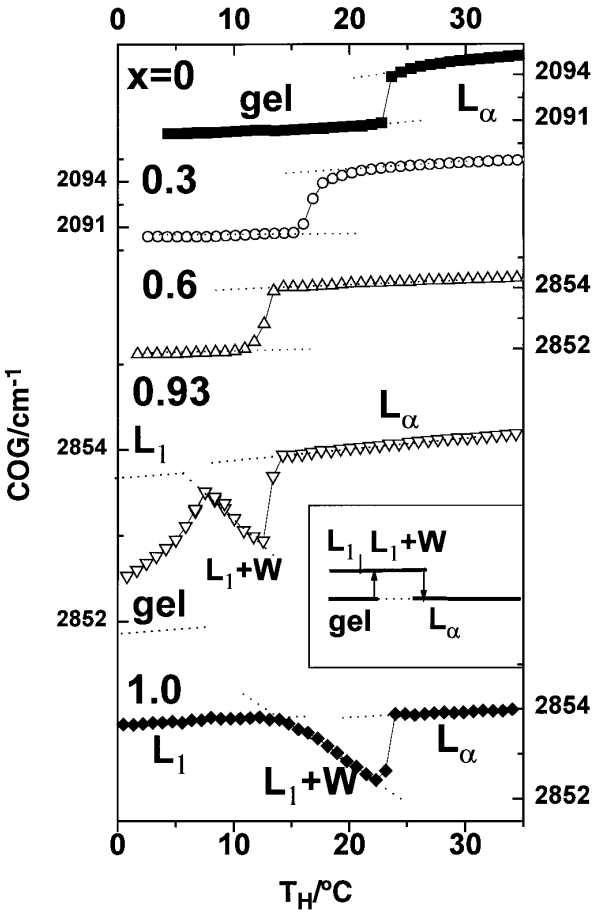

FIG. 4. The center of gravity (COG) of the symmetric methylene stretching vibration in $C_{12}E_4$/DMPC-d_{54} mixtures at different mole fractions of the surfactant, x, as a function of temperature, T_H, corresponding to the fully protonated system (cf. Eq. [4]). The $\nu_s(CD_2)$ mode of the lipid or the $\nu_s(CH_2)$ mode of the surfactant is shown in the lipid-dominated (x = 0, 0.3) or surfactant-dominated (x = 0.6, 0.93, 1) mixtures, respectively. The dotted lines extrapolate the courses of the COG beyond the phase borders. At $x = 0.93$ the L_1 and gel lines are taken from the $x = 1$ and 0.6 systems, respectively. The inset illustrates schematically the phase sequence at $x = 0.93$ (see text).

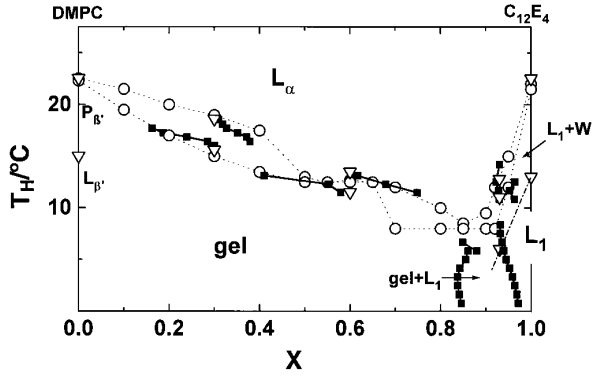

FIG. 5. Phase transition ranges of the pseudobinary mixture DMPC/$C_{12}E_4$ obtained from DSC and FTIR measurements. DSC onset and completion temperatures (○); phase border lines calculated by means of Eq. [3] using the temperature dependence of the $COG(\nu_s(CH_2))$ and $COG(\nu_s(CD_2))$ in the phase transition ranges (■); FTIR transition temperatures (▽) of the sequences $L_{\beta'}$–$P_{\beta'}$–L_α ($x = 0$), gel–L_α (0.3, 0.6), and L_1–(L_1 + W)–L_α (0.93, 1). Notations of the phase labels are given in the legend to Fig. 10.

the fluid domains contain a higher amount of surfactant than the coexisting solid domains, indicating slight deviations from ideal mixing of the components. Note that the nearly vanishing slopes of the solidus and liquidus lines in the intermediate x range imply this behavior as well.

Besides the COG shift, the melting transition of the hydrocarbon chains is marked by a drastic broadening of the CH_2 and CD_2 stretching bands (36, 37) (Fig. 7). Comparison of the bandwidths at $T = \text{const} > T_{Pt}$ reveals that the width of the $\nu_s(CD_2)$ band of the lipid decreases with x whereas the bandwidth of the $\nu_s(CH_2)$ band of the surfactant slightly increases (Fig. 7; see arrows). Interestingly, the COGs of corresponding methylene stretching bands show the opposite tendency; i.e., $COG(\nu_s(CD_2))$ of the lipid increases whereas $COG(\nu_s(CH_2))$ of the surfactant decreases with x (Figs. 8a, 8b).

A linear correlation between the degree of conformational ordering of the hydrocarbon chains and the COG of the $\nu_s(CH_2)$ band was revealed empirically in several lipid systems investigated in the liquid crystalline phase (38). Thus, the composition dependencies of the COGs of the $\nu_s(CD_2)$ and $\nu_s(CH_2)$ bands could be interpreted by the tendency of the surfactant to decrease the degree of conformational order of the lipid acyl chains, on the one hand, and to increase the packing density of the dodecyl chains of $C_{12}E_4$, on the other hand. Recently it was, however, shown that isotopic dilution shifts the methylene stretching bands toward high frequencies without variation of the conformational order (39). The increases of the $COG(\nu_s(CD_2))$ (with increasing x) and of the $COG(\nu_s(CH_2))$ (with decreasing x) correlate with the decreasing amount of the protonated and deuterated component in the mixed membranes, respectively, and thus should be attributed first to isotopic dilution and not to changes of the conformational order of the hydrocarbon chains.

Changes of the widths of the $\nu_s(CD_2)$ and $\nu_s(CH_2)$ bands are caused predominantly by intramolecular factors, including *trans*/*gauche* isomerization and librotorsional mobility (39, and references cited therein). Hence, a broadening of the methylene stretching bands can be explained by the increase of the conformational disorder of the hydrocarbon chains. Note that isotopic dilution does not affect the bandwidth significantly because it modifies intermolecular vibrational coupling only. Recent X-ray diffraction measurements on the area requirement of the compounds in mixed $C_{12}E_4$/POPC membranes at low surfactant concentrations ($x < 0.3$) suggest the tighter packing of the lipid with respect to the pure system whereas, on the other hand, the packing of the surfactant seems to loosen (2). These tendencies are expected to induce bandwidth changes of the $\nu_s(CD_2)$ and $\nu_s(CH_2)$ modes as were really observed.

Carbonyl and phosphate groups. At the chain melting transition the $\nu(C{=}O)$ band of DMPC shifts toward lower wavenumbers (cf. Fig. 8c). This behavior was typically found in aqueous dispersions of phosphatidylcholines (29, 37, 40–42) and attributed to a multicomponent nature of the C=O absorption band. It was suggested that high- and low-frequency subbands originate from populations of free and hydrogen-bound ester carbonyl groups, respectively, which explains the bandshift measured at the main transition by the relative increase of the fraction of hydrated C=O groups. A similar tendency is observed at the pretransition of the pure DMPC-d_{54} system. Note that at $x = 0.3$ the COG($\nu(C{=}O)$) starts to decrease 6–5K below the chain melting temperature (see small arrows in Fig. 8c).

Below as well as above the main transition temperature the COG($\nu(C{=}O)$) shifts upward with increasing x. Obviously, the surfactant causes the partial dehydration of the carbonyl groups or a reduction of the water accessibility in the gel as well as in the liquid-crystalline phase. This finding is in agreement with the results of previous NOESY (3),

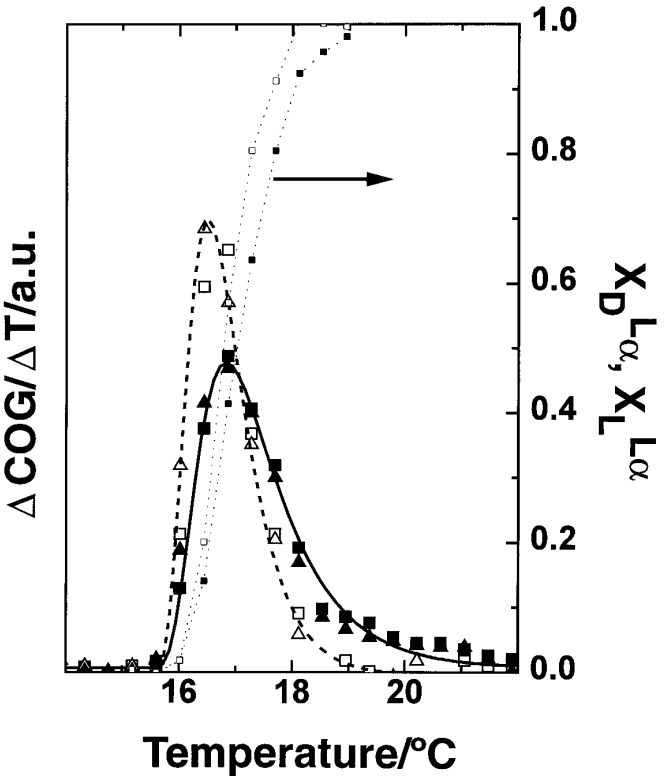

FIG. 6. First derivative of COG of the symmetric methylene stretching band in $C_{12}E_4$/DMPC-d_{54} at $x = 0.3$ as a function of temperature. The derivatives corresponding to the lipid ($\nu_s(CD_2)$, full symbols) and the surfactant ($\nu_s(CH_2)$, open symbols) are plotted for heating (squares) and cooling (triangles) scans in steps of 0.5 K. Lines are drawn for clarity. The right ordinate refers to the corresponding surfactant mole fraction of lipid and surfactant transformed to the L_α phase (cf. Eq. [2]).

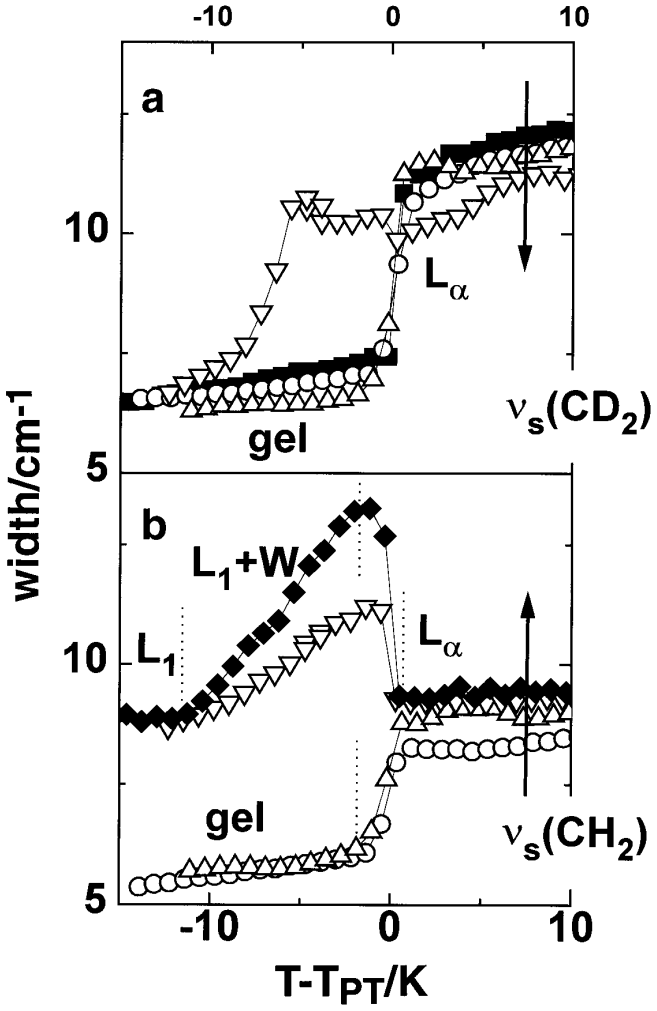

FIG. 7. Temperature dependence of the widths of the $\nu_s(CD_2)$ (a) and $\nu_s(CH_2)$ (b) vibration bands of the lipid and surfactant, respectively, in systems of surfactant mole fractions: $x = 0$ (○), 0.3 (□), 0.6 (△), 0.93 (▽) and 1 (◆). The temperature scale was shifted relative to phase transition temperatures, T_{PT}, corresponding to the gel–L_α ($x < 0.9$) and to the (L_1 + W)–L_α ($x > 0.9$) transitions. The arrows indicate changes with increasing x.

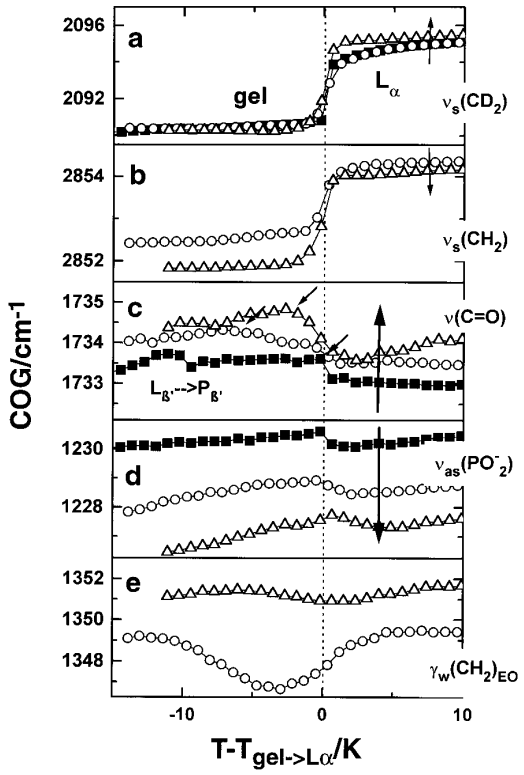

FIG. 8. The center of gravity of selected IR-absorption bands in $C_{12}E_4$/DMPC-d_{54} systems of surfactant mole fractions $x < 0.7$: $x = 0$ (○), 0.3 (□), 0.6 (△) as a function of temperature. The temperature scale was shifted relative to the gel–L_α phase transition temperature indicated by the vertical dotted line. The vertical arrows illustrate changes with increasing x. The small arrows in c indicate the onset of the COG drop (see text).

gravimetrical (2), and ITC (43) studies on POPC/$C_{12}E_4$ mixtures where the ethoxy groups are suggested to replace the water in the headgroup region of the bilayer partially.

It is widely accepted that the frequency of the $\nu_{as}(PO^-_2)$ vibration is very sensitive to lipid hydration, mainly because of direct H-bonds between water and the charged phosphate oxygens (40, 44–46). Hence, the downward shift of the COG of the $\nu_{as}(PO^-_2)$ mode monitors the increasing hydration of the phosphate group at the chain melting transition in a fashion similar to the carbonyl group (cf. Fig. 8d).

With increasing surfactant content, however, the COG-($\nu_{as}(PO^-_2)$) indicates increasing hydration, in contrast to the carbonyl group, which is assumed to be dehydrated by the surfactant. In addition to direct water–phosphate contacts, other effects may also influence the $\nu_{as}(PO^-_2)$ band position. Theory predicts frequency shifts as a result of direct interaction of the trimethylammonium group with the phosphate, as well as a result of changes of the torsion angles of the C–O–P–O–C fragment (45). In aqueous monooleylglycerol/DOPC mixtures the hydroxylic groups of the surfactant form H-bonds to the phosphate group of the lipid (40). These interactions shift the phosphate band toward lower wavenumbers in a manner similar to that for $C_{12}E_4$/DMPC. Hence, one can suggest direct interactions between the ethoxy-hydroxyl and the phosphate groups in the system investigated.

Ethoxy chains. Crystalline polyethylene glycol dimethyl ethers show an intense, relatively narrow absorption band at about 1345 cm^{-1} originating from the antisymmetric coupling of the hybridized methylene wagging (65%) and twisting (35%) modes. It appears in the *gauche* conformation of the O–$(CH_2)_2$–O– unit only (32, 33). Upon melting, this band fuses with the corresponding symmetrical coupling mode into one broader peak at about 1350 cm^{-1} (31) found also in the spectrum of $C_{12}E_4$ under all conditions investigated in the present study (cf. Fig. 1b). It differs essentially from the respective bandshape and position of crystallized ethoxy chains as illustrated in Fig. 1b where the $\gamma_w(CH_2)_{EO}$ band of crystalline $C_{16}E_4$ is drawn for comparison. Obviously, the freezing of the alkyl chains in the surfactant/lipid mixture at the L_α–gel phase transition is not accompanied by the crystallization of the ethoxy chains. Note that crystallized ethoxy chains of C_mE_4 are assumed to adopt an extended helical conformation with the *trans–gauche–trans* sequence of the torsional angles in the O–$(CH_2)_2$–O– unit (32, 47, 48). On melting, torsional rotations occur predominantly about the C–O bonds, which have lower barriers than the C–C bands. Consequently, the *gauche* conformation of the O–$(CH_2)_2$–O– fragment remains substantially unchanged in molten and crystalline ethoxy chains, and the spectral changes of the $\gamma_w(CH_2)_{EO}$ band account for second-order effects of the ethoxy chain conformation (31).

Interestingly, in the mixed membranes the COG($\gamma_w(CH_2)_{EO}$) starts changing at considerably lower temperatures than the COG($\nu_s(CH_2)$) (cf.Fig. 8e). This effect is much more pronounced at $x = 0.3$ than at $x = 0.6$ and indicates possibly subtle modifications of the conformation of the ethoxy chains preceding the melting of the alkyl chains. On the basis of the downward shift of the $\gamma_w(CH_2)_{EO}$ band upon crystallization, we assume that the decrease of COG(γ_w-$(CH_2)_{EO}$) before melting indicates the tendency of the ethoxy chains to adopt a more stretched conformation. In the framework of this hypothesis the systematic increase of the COG-($\gamma_w(CH_2)_{EO}$) with higher surfactant content would mean that the degree of disorder of the ethoxy chains increases with x. It was shown in monooleylglycerol–water dispersions (49) that atomic groups which are located at the polar/apolar interface show pretransitional temperature induced changes similar to the behavior of the COG(ν(C=O)) and COG($\gamma_w(CH_2)_{EO}$) in the surfactant/lipid system investigated.

Micellar and Lamellar Transitions at $x > 0.7$

Hydrocarbon chains. $C_{12}E_4$ dispersed in water at low temperatures assembles into micelles (L_1 phase) (24, 25). Upon being heated, the system undergoes a second-order micellar transition from a homogeneous (L_1) to a heteroge-

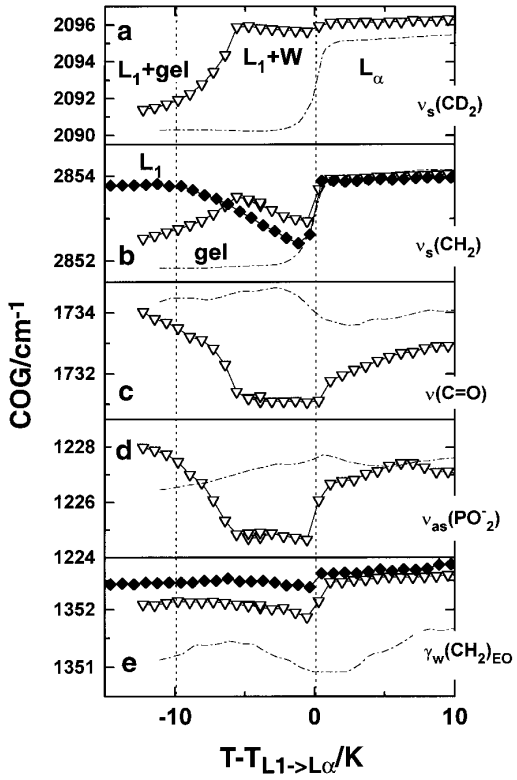

FIG. 9. The center of gravity of selected IR-absorption bands in $C_{12}E_4$/DMPC-d_{54} systems of surfactant mole fractions $x > 0.7$: $x = 0.93$ (▽) and 1 (♦) as a function of temperature. The temperature scale was shifted relative to the $(L_1 + W)-L_\alpha$ phase transition temperature. The left vertical dotted lines indicates the $(L_1 + gel)-(L_1 + W)$ or $L_1-(L_1 + W)$ transitions. The COGs for $x = 0.6$ are redrawn from Fig. 8 (dash–dotted curves) for comparison.

neous ($L_1 + W$) state (clouding phenomenon), and at $T = 22.5$°C the aggregates convert into liquid-crystalline surfactant bilayers (L_α). Inspection of the courses of the spectral parameters calculated from the $\nu_s(CH_2)$ mode indicates three typical temperature ranges which we assign accordingly to the phase sequence expected (cf. Fig. 4 at $x = 1$ and Fig. 9b, solid diamonds). In the L_1 and the L_α phases the COG($\nu_s(CH_2)$) values are very similar, whereas in the ($L_1 + W$) range in between, the COG($\nu_s(CH_2)$) decreases, accompanied by a substantial broadening of the $\nu_s(CH_2)$ band (Fig. 7b; see also Fig. 1c). Relatively broad C–H stretching bands are typically found in nonlamellar, fluid molecular aggregates (cubic, micellar) (49). The increasing bandwidth in the ($L_1 + W$) range can be attributed to an increasing degree of disorder of the hydrocarbon chains. NMR (50), ESR, and fluorescence anisotropy (11) studies on aqueous dispersions of $C_{12}E_5$ and DPPC/$C_{10}E_7$, respectively, also reveal highly disordered alkyl chains in the range of micellar phase separation.

The courses of the COG($\nu_s(CH_2)$) and of the $\nu_s(CH_2)$ bandwidth of the mixture with low lipid content ($x = 0.93$) closely resemble that of the pure surfactant system. This finding indicates an analogous phase sequence which is shifted, however, to lower temperatures (cf. Figs. 4, 7b, and 9b). Starting the heating scan more than 5 K below the ($L_1 + W$)-L_α transition temperature, $T_{L1-L\alpha}$, increases the COG($\nu_s(CH_2)$) in contrast to the pure surfactant system (Fig. 9b). The sigmoidal courses of the COG and of the width of the $\nu_s(CD_2)$ mode in this temperature range resemble the respective changes observed at the gel–L_α transition, and thus should be attributed to the melting of the lipid acyl chains (cf. Figs. 7a and 9a). Consequently, at low temperatures lipid-enriched gel-state lamellae are assumed to coexist with surfactant-rich micelles, in contrast to the pure surfactant/water system. Upon heating, the membranes completely solubilize into mixed micelles accompanied by the melting of the hydrocarbon chains, as illustrated schematically in the insert given in Fig. 4.

The existence of the heterogeneous micellar ($L_1 + W$) phase in the lipid/surfactant mixture just below $T_{L1-L\alpha}$ can be deduced from the decreasing COG($\nu_s(CH_2)$) (Fig. 9b at $-5\ K < (T - T_{L1-L\alpha}) < 0\ K$) and from the distinct broadening of the absorption band (Fig. 7b at $-10\ K < (T - T_{L1-L\alpha}) < 0\ K$). Both effects are observed in the ($L_1 + W$) phase range of the pure surfactant system and thus their appearance give evidence of the existence of the heterogeneous micellar phase in the mixture at $x = 0.93$ as well.

The solidus and liquidus lines (i.e., the boundaries of the coexistence ranges) are calculated for the transitions L_1–gel, ($L_1 + W$)–gel, and ($L_1 + W$)–L_α by means of Eqs. [2] and [3] using the COGs of the methylene stretching modes for $x = 0.93$ and the respective values measured at $x = 1$ and $x = 0.6$ as reference data for the pure micellar and gel phases, respectively (cf. Fig. 4). This choice yields only crude estimates for the micellar–gel boundaries. First, the course of the COG($\nu_s(CD_2)$) in mixed micelles is not known precisely. Second, the differentiation between the fractions of the lipid or detergent which belong to the micellar or lamellar phases by means of the center of gravity is not very precise because of the broad methylene stretching bands. The attempt to decompose the absorption bands into subbands which correspond to the gel and fluid component yields results almost similar to those obtained from the COGs (data not shown). Note that the use of band separation techniques does not overcome the problems mentioned above. For example, the broad $\nu_s(CH_2)$ band of pure $C_{12}E_4$ in the ($L_1 + W$) phase shown in Fig. 1c can be approximated in a satisfactory (but wrong) fashion by the superposition of the respective bands measured in the L_α (or L_1) and gel states.

The integral intensity of the $\nu_s(CH_2)$ band drops in the ($L_1 + W$) range by more than 50%. Despite the spectral weighting factor g_1/g_2 in Eq.[2], we suppose that in the ($L_1 + W$)–gel coexistence range our algorithm overestimates the fraction of surfactant molecules situated in gel-state membranes and thus shifts the respective left-hand phase

boundary to greater x. Note that, on the other hand, the width of the $\nu_s(CH_2)$ band at $x = 0.93$ gives no indication of $C_{12}E_4$ with frozen alkyl chains (Fig. 7b).

Polar groups. When the mixture with the high surfactant content ($x = 0.93$) is heated, the COG of the carbonyl stretching band, COG(ν(C═O)), decreases continuously to a minimum followed by a slow increase (cf. Fig. 9c) and thus deviates considerably from its behavior at $x < 0.7$. The drop of COG(ν(C═O)) is in accordance with the solubilization of the lipid lamellae into mixed micelles, where the positive curvature of the micellar surface causes a stronger exposure of the carbonyl groups to the water. Note that in contrast to this behavior inverse lipid aggregates (e.g., H_{II}) are characterized typically by the partial dehydration of the carbonyl group evidenced by a shift of the ν(C═O) band in the opposite direction (36). An increase of the COG(ν(C═O)) starts in the system investigated at $T_{L1-L\alpha}$, where it indicates, however, the $(L_1 + W)-L_\alpha$ phase transition followed by the continuous dehydration of the carbonyl group in the mixed bilayers with increasing temperature. The relatively small absolute values of the C═O band frequency suggest that the carbonyl moiety is hydrated more strongly in the surfactant enriched bilayers than in the lipid dominated lamellae. Pyrene fluorescence also indicates a local drop in polarity at the polar/apolar interface at the micellar–lamellar transition of aqueous mixtures of $C_{10}E_7$/DPPC (11).

The course of the COG($\nu_{as}(PO_2^-)$) shows that the changes of hydration in the vicinity of the carbonyl group also extend to the phosphate group (cf. Fig. 9d). Obviously, the curved polar/apolar interface of the micellar aggregates increases the hydration of the phosphate group as well. The $\gamma_w(CH_2)_{EO}$ are not sensitive to the micellar clouding but shift at the $(L_1 + W)-L_\alpha$ transformation (cf. Fig. 9e).

DISCUSSION

Phase Behavior

The data obtained from DSC and FTIR measurements combined with the knowledge of the amphotropic phase behavior of the DPPC/$C_{12}E_4$ system (12) allows us to construct the pseudobinary phase diagram represented in Fig. 10. The phase regions are labeled by following the notation of Luzatti and Tardieu (51).

The coexistence of the rippled phase $P_{\beta'}$, the gel phase $L_{\beta'}$, and the liquid crystalline phase as a peritectic point at $x = 0.1$ is speculative and based on the assumption that this system obeys the Gibbs phase rule. But a critical phase line might also be conceivable (cf. inset to Fig. 10) along with the ripple phase $P_{\beta'}$ and the adjacent gel phase ($L_{\beta'}$ or L_β) cannot be distinguished by means of DSC and FTIR. One can suppose that the long distance periodical superstructure of the ripple phase $P_{\beta'}$ is gradually disturbed with the accumulation of assimilated surfactant and finally becomes identical

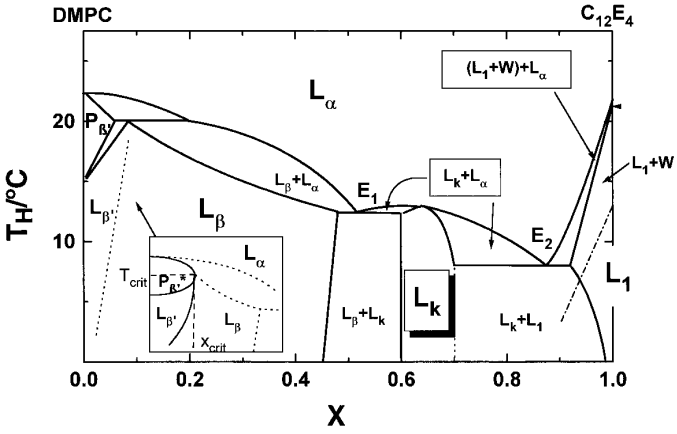

FIG. 10. Phase diagram of the pseudobinary mixture DMPC/$C_{12}E_4$. Phase boundaries are drawn by solid, dash–dotted (clouding: $L_1-(L_1 + W)$), or dotted (relative high uncertainty or hypothetical) lines. The phase labels follow the Luzatti notation: L_α, lamellar liquid crystalline phase; L_β, lamellar gel phase with nontilted hydrocarbon chains; $L_{\beta'}$, lamellar gel phase with tilted chains; $P_{\beta'}$, ripple phase; L_k lamellar gel compound complex; L_1, homogeneous micellar phase; $(L_1 + W)$, heterogeneous micellar + water phase (clouded); E_1, E_2, eutectic points). Inset: Modified phase diagram with critical behavior between $P_{\beta'}$, $L_{\beta'}$, L_β, and L_α. at $x < 0.1$.

to the nonrippled lamellar gel phase ($L_{\beta'}$ or L_β). This behavior corresponds to liquid/vapor coexistence at the critical temperature (or pressure respectively) at which thermodynamic and structural properties of both phases approach. In our pseudobinary system the peritectic point would be reduced in this case to an imaginary one and the phase boundary of $P_{\beta'}$ forms a closed phase line with critical behavior, i.e., without coexistence ranges. The same can be assumed for the phase boundary between $L_{\beta'}$ and L_β (Fig. 10 insertion, solid line). The shrinking of the DSC pretransition enthalpy between $x = 0$ and $x = 0.1$ corroborates this hypothesis.

A tilt of the hydrophobic chains seems to be unlikely for higher amounts of surfactant because both components are expected to match well in molecular length due to the identical number of methylene units per hydrocarbon chains. Consequently, a boundary between the $L_{\beta'}$ and L_β phases is expected but could not, however, be accurately determined by the methods used (dotted line in Fig. 10). From a thermodynamic and conformational point of view, the L_β phase of the mixture does not drastically differ from the pure lipid lamellar $L_{\beta'}$ phase (26). The single phase regions L_β and $P_{\beta'}$ represent solid solutions where the surfactant is dissolved in the lipid matrix.

The linear decrease of the lipid main phase transition enthalpy, the lowering of T_m, and the relatively narrow DSC curves indicate almost ideal mixing between $x = 0$ and 0.5. Up to this surfactant fraction the mixing properties seem to be determined mainly by the hydrocarbon chains of equal length in the same manner as, for example, in the case of binary mixtures of lipids with long chain alcohol or their derivatives (16, 17).

The collapse of the DSC transition width to 2 K at a molar mixing ratio of 1:1 ($x = 0.5$) DMPC and $C_{12}E_4$ points out a drastic change in the lateral arrangement of the components compared to mixtures with less surfactant. Up to $x = 0.65$, the transition range remains very narrow, resembling the melting of a one-component system which is assumed to be caused by the formation of a surfactant–lipid complex in the gel state, L_k. The broadening of the DSC peak with further increasing surfactant concentration ($x = 0.65 - 0.7$) indicates demixing in the gel phase. Following the Gibbs phase rule two eutectic points at $x \cong 0.5$ and 0.9 are expected (E_1 and E_2 in Fig. 10), where lipid and surfactant constitute a mixture which melts like a pure substance. E_2 is experimentally indicated by the sharp DSC endotherm, which is, however, superimposed by phase transitions of higher order on the low temperature side (cf. Fig. 2). From thermodynamic considerations the formation of the compound complex (denoted as L_k) between these two eutectic mixtures is inevitable. At composition below or above $x = 0.66$, the pseudobinary system can be viewed as a solid solution of the complex (mole ratio DMPC/$C_{12}E_4$ = 1:2) uniformly mixed with either excess DMPC or excess $C_{12}E_4$, respectively. Based on X-ray and NMR studies (52), L_k has an L_β structure.

Taking into account the FTIR data measured at $x = 0.93$, we assume a two-phase region at $0.85 < x < 0.95$ and $T < 8$°C which consists of a lamellar gel complex DMPC/$C_{12}E_4$ in equilibrium with highly $C_{12}E_4$-enriched fluid micelles. With the surfactant mole fraction x, the population of mixed micelles (L_1 in Fig. 10) increases and that of the lamellar complex L_k decreases (*Lever rule*). L_k disappears slightly above $x = 0.9$. The infrared spectra indicate the parallel melting of the hydrocarbon chains of the lipid and of the surfactant already below 8°C. Hence, the low-temperature shoulder of the DSC peaks should be attributed partially to the first-order chain melting transition appearing upon solubilization of L_k lamellae. Solubilization reduces the amount of mixed bilayers and, therefore, the right ($L_1 + L_k$)–L_1 phase boundary changes with x (Fig. 10). In view of the relative high uncertainty of the left boundary of ($L_1 + L_k$) coexistence drawn in Fig. 5 and taking into consideration that the low-temperature shoulder of the DSC peaks already appears at $x > 0.7$, we shift the $L_k - (L_1 + L_k)$ phase boundary down to $x = 0.7$.

The phase behavior of DMPC/$C_{12}E_4$ at $x > 0.7$ closely resembles that of the related pseudobinary mixtures DPPC/$C_{12}E_4$ (12) and $C_{10}E_n$/PC ($n = 5–7$, PC: DMPC, DPPC, DSPC) (9, 10). Only a slightly decreased eutectic temperature in DMPC/$C_{12}E_4$ (9°C) could be observed compared to DPPC/$C_{12}E_4$ (15°C), where the longer palmitoyl chains increase the melting temperature. In the latter system the complex decomposes before melting, in contrast to DMPC/$C_{12}E_4$. The increased alkyl chain length of $C_{12}E_4$ in comparison with that of $C_{10}E_4$ causes the preferential formation of lamellar structures and thus extents the concentration range of the mixed lamellar phase toward higher surfactant content and lower temperature. In other words $C_{12}E_4$ solubilizes the membranes only at high surfactant concentration and at low temperatures when compared with $C_{10}E_n$/PC systems (9, 10).

Alternatively to micelle–bilayer (gel) coexistence Inoue *et al.* (11) suggest surfactant-enriched $C_{10}E_7$/DPPC mixed disk-like micelles where frozen and fluid hydrocarbon chains are separated into bilayer-like areas in their centers and curved regions at their edges, respectively. The composition-dependent DSC endograms presented in Refs. (9) ($C_{10}E_7$/DMPC) and (19) ($C_{10}E_7$/DPPC) show features similar to those of the endograms presented in Fig. 2. Hence, these data give indication of the existence of a gel compound complex at about $x = 0.35–40$ in both cases, in qualitative agreement with our results. We conclude that the micelle–complex coexistence range ($L_1 + L_k$) drawn in Fig. 10 refers to properties of the system similar to those of the range of mixed micelles assumed in Refs. (9, 10).

At low temperatures the micelles are homogeneously dispersed within the sample (L_1 in Fig. 10). When the temperature is raised, the hydrophilicity of the ethoxy groups shrinks and the micelles tend to separate from bulk water ($L_1 + W$ in Fig. 10), generating the *cloud point* phenomenon, which is indicated by a significant baseline shift in the DSC endograms and by characteristic changes of infrared absorption bands. Temperature- and composition-driven second-order transitions are known to occur in pure and mixed micelles, where the presence of the lipid component usually reduces the clouding temperature considerably (9, 53, 54). The incorporation of DMPC into $C_{12}E_4$ micelles decreases the cloud point temperature by 10 K at $x = 0.93$.

The sharp but low-enthalpic DSC peaks measured at $x > 0.9$ and $T < 22$°C indicate the transition from the mixed micellar ($L_1 + W$) phase to the lamellar liquid crystalline phase L_α, analogous to the phase behavior of pure $C_{12}E_4$/water (24, 25). The high-temperature lamellar- to nonlamellar-phase transitions ($T > 60$°C) observed at high concentrations of $C_{12}E_4$ ($x > 0.8$) are not considered in our phase diagram. They are in close agreement with similar transitions observed in the pseudobinary system DPPC/$C_{12}E_4$ at excess water and in the pure $C_{12}E_4$/water dispersion.

We summarize that the combination of DSC with FTIR measurements yields complementary information about the thermotropic phase behavior of lipid/nonionic surfactant mixtures at excess water. Nevertheless, some boundaries at low temperature remain speculative (dashed lines in Fig.10). Intersections of phase boundaries are drawn in accordance with the Gibbs phase rule, which predicts for a binary system at maximum three phases in thermodynamic equilibrium. The coexistence of ($L_1 + W$), L_k, and L_α at the eutectic point E_2, i.e., of four phases, seems to contradict the Gibbs phase rule. However, in this range the aqueous component is strongly involved in the phase behavior and consequently the assumption of a pseudobinary system is not valid.

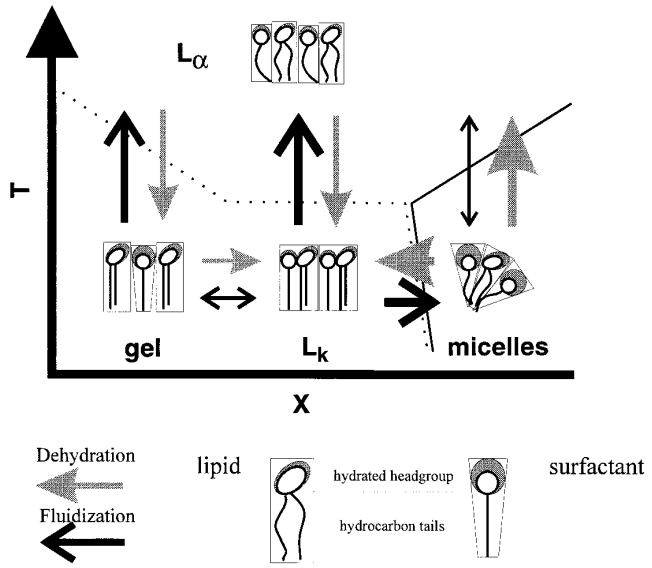

FIG. 11. Schematic illustration of structural changes associated with the phase transitions in C_mE_n/PC pseudobinary mixtures. Chain melting transition and bilayer solubilization are marked by dotted and full lines, respectively. The arrows are drawn in direction of decreasing hydration of the lipid headgroup and increasing conformational disorder of the hydrocarbon chains. Both effects are endotherm. The double arrows indicate small effects.

Structure and Heat Effects

The formation of supermolecular aggregates of amphiphiles can be treated in terms of the molecular shape concept (55) or by means of spontaneous curvature in the frame of the membrane elasticity model (56). Surfactants of the type $C_{12}E_m$ are characterized by the shape of a truncated cone, cylinder, or inverse cone (7, 43, 57) where the lateral area occupied by the hydrated headgroup in an aggregate is larger than, equal to, or even smaller than the optimum interfacial area per hydrocarbon chain, respectively. Fully hydrated $C_{12}E_4$ at room temperature assembles into surfactant lamellae (L_α) and therefore can be assumed to adopt a cylindrical shape. Consequently, the surfactant is in a good match with the lipid, which also can be imagined as a cylindrical molecule due to its bilayer-forming potency. Upon mixture both components assemble into mixed bilayers with a negligible spontaneous curvature at all.

In terms of molecular properties two effects, namely hydration of the polar head groups and fluidity of the hydrocarbon chains, can modulate the molecular shape of the constituents and thus the morphology of the aggregates (Fig.11). For example, with decreasing temperature the area occupied by the hydrocarbon chains within the membranes is reduced due to the increasing conformational order of the methylene segments. Furthermore, with decreasing T the strongly hydrophilic ethoxy chains hydrate and therefore tend to occupy an increased area within the hydrophilic interface. These effects cause a curvature strain which favors the formation of mesophases with high positive curvature like micelles (L_1), which are really observed in $C_{12}E_4$/DMPC at $x > 0.7$ and low temperatures (right low corner in Fig.11). The presence of the lipid in mixed micelles, on the other hand, reduces their spontaneous curvature in comparison with pure ones. As a consequence, the mixed micelles transform to lamellae at lower temperatures, i.e., at higher level of hydration of the ethoxy chains. Thus the solubilization of the fluid membranes (L_α–micelle transformation) can be triggered by temperature and composition.

Changes of the conformation and packing of the hydrocarbon chains (fluidity) and of headgroup hydration are accompanied by enthalpy changes and, consequently, represent the main sources of the transition enthalpies measured. According to a model which was previously established by Kjellander (58) on the basis of theoretical studies of polyethylene oxide/water systems (59), water molecules interact through hydrogen bonding to the ether oxygens of $C_{12}E_4$. This leads to hydration shells where the structure of water shows a higher order, as in bulk water. The interaction between two ethoxy chains is dominated by the effect of overlapping hydration shells, leading to the release of water. This effect is associated with positive enthalpy and entropy changes (60) and therefore the interaction between the hydration shells of different ethoxy chains is repulsive at low temperatures (hydration yields enthalpy gain) but becomes attractive at higher temperatures (dehydration yields entropy gain) when the entropy term dominates the thermodynamics.

If one assumes that these temperature effects will be the same for intra- as for intermicellar interactions, the decreased repulsion between the ethoxy chains results first in an increased tendency of the micelles to aggregate (L_1–(L_1 + W) transformation) and subsequently leads to the formation of lamellar structures with a reduced area requirement per polar ethoxy group ((L_1 + W)–L_α transition) (60). Upon the thermotropic micelle–bilayer transformation at high surfactant content, FTIR indicates that the phosphate and carbonyl groups of DMPC dehydrate and the fluidity of the alkyl chains of the surfactant decreases slightly. Thus the corresponding measured endothermic transition heat can be attributed mainly to the dehydration of the polar interface and not to chain ordering (exotherm). It was found previously that the variation of hydration in $C_{12}E_n$/lipid systems itself can cause considerable enthalpic effects at room temperature (43), in contrast to simple hydrocarbons (62). On the other hand, in the lipid-dominated bilayer range ($x < 0.5$), ΔH originates almost exclusively from the melting of the hydrophobic polymethylene chains.

Recent calorimetric studies revealed the existence of surfactant/lipid complexes in the gel states $C_{10}E_7$/PC (9, 10) and $C_{12}E_4$/DPPC (12) mixed bilayers which are suggested to be caused by an optimal sterical matching of both components. The DSC data give evidence of a $C_{12}E_4$/DMPC complex with a stochiometric ratio of about 2:1 appearing in the

intermediate concentration range. It includes slightly more surfactant than $C_{12}E_4$/DPPC (3:4) (12) and $C_{10}E_7$/PC (3:4) (9, 10). Also, ITC solubilization investigations on fluid $C_{12}E_4$/POPC mixed bilayers (43) indicate enthalpically preferred interactions in surfactant–lipid clusters which can be viewed as one prerequisite of the complex formation observed in the rigid bilayers.

How can we explain the formation of a stable lamellar gel complex with optimized chain packing even though the surfactant destabilizes the lipid gel phase at low x. The complex formation is induced, obviously, by the replacement of water from the headgroup region leading to direct lipid/surfactant headgroup interactions which improve the molecular packing and thus strengthen the van der Waals interactions between the hydrocarbon chains. Our results indicate an interaction between the ethoxy–hydroxyl and lipid phosphate groups and the surfactant-induced dehydration of the carbonyl group of DMPC. This position was found to affect the molecular arrangement in an exceptionally sensitive manner because of its pivotal location near the polar/apolar interface (61). Due to the maximum number of lipid/surfactant contacts the complex demixes in a separate phase in the intermediate x range.

The marked decrease of the COG(ν(C═O)) at the gel–L_α transition of the mixed bilayer in the range of complex existence was interpreted in terms of graded water invasion into the carbonyl region (cf. Fig. 8c). Hence, the partial destruction of L_k during the phase transition leads to increased hydration of the headgroup region of the bilayer. However, this effect is expected to release heat and thus cannot explain the higher incremental transition heats determined for the melting of the complex. Consequently, the increase of the incremental transition enthalpy by more than 50% (Fig. 3, open triangles) in the range $x = 0.5–0.7$ should be interpreted as an indication of stronger attractive interactions between the components in the gel phase complex. The partial destruction of the complexes at the melting transition should consume heat and thus appears as the gradual increase of the DSC transition heat in agreement with our findings.

ITC yields an exothermic net heat in the order of 1–2 kJ/mol (of surfactant), which results from lipid–surfactant aggregation after transfer of surfactant from pure surfactant into mixed bilayers (43). Note that the indication of surfactant/lipid pairs in fluid membranes is related to enthalpically favored molecular configurations between adjacent surfactant and lipid molecules within a homogeneous phase of an almost statistical distribution of the components. The DSC data reveal the separation of the system into gel + gel and gel + fluid coexistence ranges, i.e., into aggregates (e.g., $L_k + L_1$) and/or domains (e.g., $L_k + L_\beta$, $L_k + L_\alpha$) of different composition. Relating the additional complex formation heat of about 4–5 kJ/mol (of surfactant + lipid) in the mixture ($x \approx 0.5–0.7$) to the surfactant only, one obtains a net contribution of about 7–10 kJ/mol (of surfactant). This value exceeds the respective net enthalpy for fluid membranes by nearly one order of magnitude and therefore explains the high stability of gel state complexes. In the rigid state collective effects, such as the effective packing of the hydrocarbon chains within crystalline subcells or chain interdigitation, can induce closer intermolecular spacings than in the fluid state, which would cause stronger interactions between the molecules (52).

In the present system the complex remains stable up to the melting transition temperature, whereas in $C_{12}E_4$/DPPC mixed bilayers the complex decomposes slightly below its expected melting point (12). Possibly, the identical number of methylene units per hydrocarbon chain in $C_{12}E_4$ and DMPC causes the optimal fit between the dodecyl and the myristoyl chains and thus higher L_k stability in contrast to the longer palmitoyl chains. On the other hand, the pronounced dependence of hydration of the ethoxy chains on the absolute temperature (13, 14, 43) may cause destabilization of the gel complex at higher temperatures, which are reached in DPPC but not in DMPC membranes due to the lower chain melting temperature T_m.

CONCLUSIONS

The phase diagram obtained for aqueous dispersions of DMPC/$C_{12}E_4$ is qualitatively in good agreement with that obtained for DPPC/$C_{12}E_4$ dispersions. In general, the pseudobinary mixture of fully hydrated disaturated PCs and $C_{12}E_4$ shows the following properties:

—Addition of the surfactant to lipid-dominated bilayers (low x) destabilizes the gel phase and thus reduces the chain melting transition temperature

—Addition of lipid to surfactant-dominated micelles (high x) destabilizes the micellar aggregates and thus reduces the micellar–lamellar transition temperature.

—A wide range of temperatures (room temperature and higher) and concentrations is occupied by the lamellar liquid crystalline phase.

—In the intermediate concentration range a compound complex stabilizes the gel state bilayers; i.e., it stops the further reduction of the gel–L_α and L_1–L_α transition temperatures with increasing and decreasing x, respectively.

—Excess amounts of surfactant or lipid are strongly phase separated from the complex in the concentration ranges adjacent to complex composition.

—Almost ideal mixing of the surfactant with the lipid at low x is promoted by hydrocarbon chains of equal length in the lipid and surfactant.

—In qualitative agreement with hydrated PC/$C_{10}E_7$ mixtures (9, 10) the solubilization of mixed $C_{12}E_4$ rich lamellae into mixed micelles is also mostly determined by the order–disorder transition of the PC acyl chains and thus can be triggered by temperature.

FTIR spectroscopy turns out to complement the calorimetric results on lipid/surfactant mixtures in three respects:

(i) The combination of deuterated and protonated components allows the chain melting of each component to be followed separately and in this way the phase boundaries to be constructed in a wide concentration range.

(ii) FTIR appears to be more sensitive to structural conversions with only weak enthalpic output such as second-order phase transitions (e.g., micellar transition) and smeared chain melting (e.g., solubilization in the L_k–L_1 coexistence range).

(iii) Spectroscopic results can be interpreted in terms of semiempirical parameters which are correlated to effects such as hydration or the conformation of different atomic groups (e.g., acyl chains). Consequently, FTIR yields information about the molecular background of phase transformations.

The formation of a compound complex in the gel state is accompanied by a substantial enthalpy gain. Despite indications of dehydration of the polar region of the bilayer and tightening of the packing of the hydrocarbon chains, the detailed structure of the compound complex is not clear yet.

ACKNOWLEDGMENT

We gratefully acknowledge the Deutsche Forschungsgemeinschaft for the financial support in the framework of SFB 294/C7.

REFERENCES

1. Volke, F., Eisenblätter, S., Galle, J., and Klose, G., *Chem. Phys. Lipids* **70,** 121 (1994).
2. König, B., Dietrich, U., and Klose, G., *Langmuir* **13,** 526 (1997).
3. Volke, F., and Pampel, A., *Biophys. J.* **68,** 1960 (1995).
4. Dennis, E. A., *Arch. Biochem. Biophys.* **165,** 764 (1974).
5. Naumann, C., Dietrich, C., Lu, J. R., Thomas, R. K., Rennie, A. R., Penfold, J., and Bayerl, T. M., *Langmuir* **10,** 1919 (1994).
6. Klose, G., Islamov, A., König, B., and Cherezov, V., *Langmuir* **12,** 409 (1996).
7. Lantzsch, G., Binder, H., Heerklotz, H., Wendling, M., and Klose, G., *Biophys. Chem.* **58,** 289 (1996).
8. Heerklotz, H., Binder, H., Lantzsch, G., and Klose, G., *Biochim. Biophys. Acta* **1196,** 114 (1994).
9. Inoue, T., Motoyama, R., Totoki, M., Miyakawa, K., and Shimozawa, R., *J. Colloid Interface Sci.* **164,** 318 (1994).
10. Inoue, T., Motoyama, R., Miyakawa, K., and Shimozawa, R., *J. Colloid Interface Sci.* **156,** 311 (1993).
11. Inoue, T., Kawamura, H., Okukado, S., and Shimozawa, R., *J. Colloid Interface Sci.* **168,** 94 (1994).
12. Mädler, B., Klose, G., Möps, A., Richter, W., and Tschierske, C., *Chem. Phys. Lipids* **71,** 1 (1994).
13. Funari, S., and Klose, G., *Chem. Phys. Lipids* **75,** 145 (1995).
14. Klose, G., Eisenblätter, S., and König, B., *J. Colloid Interface. Sci.* **172,** 438 (1995).
15. König, B., and Klose, G., *Progr. Colloid Polym. Sci.* **93,** 279 (1993).
16. Schullery, S. E., Seder, T. A., Weinstein, D. A., and Bryant, D. A., *Biochemistry* **20,** 6818 (1981).
17. Gawrisch, K., and Holte, L. L., *Chem. Phys. Lipids* **81,** 105 (1996).
18. Strey, R., Schomäcker, R., Roux, D., Nallet, F., and Olsson, U., *J. Chem. Soc. Faraday Trans.* **86,** 2253 (1990).
19. Lukaschek, M., Müller, S., Hansenhindl, A., Grabowski, D. A., and Schmidt, C., *Colloid Polym. Sci.* **274,** 1 (1996).
20. Lukaschek, M., Grabowski, D. A., and Schmidt, C. *Langmuir* **11,** 3590 (1995).
21. Eytan, G. D., *Biochim. Biophys. Acta* **694,** 185 (1982).
22. Levy, D., Gulik, A., Seigneuvet, M., and Rigaud, J.L., *Biochemistry* **29,** 9480 (1990).
23. Zumbuehl, O., and Weder, H. G., *Biochim. Biophys. Acta* **640,** 252 (1981).
24. Tiddy, G. J. T., *Phys. Rep.* **57**(1), 1 (1980).
25. Mitchel, D. J., Tiddy, G. J. T., Warning, L., Bostock, T., and McDonald, M. P., *J. Chem. Soc. Faraday Trans. 1* **79,** 975 (1983).
26. Mantsch, H. H., Cameron, D. G., Tremblay, P. A., and Kates, M., *Biochim. Biophys. Acta* **689,** 63 (1982).
27. Lee, D., Durrani, A., and Chapman, D., *Biochim. Biophys. Acta* **769,** 49 (1984).
28. Laroche, G., Carrier, D., and Pezolet, M., *Biochemistry* **27,** 6220 (1988).
29. Blume, A., Hübner, W., and Messner, G., *Biochemistry* **27,** 8239 (1988).
30. Dörfler, H. D., Brezesinski, G., and Miethe, P., *Chem. Phys. Lipids* **48,** 245 (1988).
31. Davidson, W. H. T. *J. Chem. Soc.* **51,** 3270 (1955).
32. Miyazawa, T., Fukushima, K., and Ideguchi, Y., *Journal of Chem. Physics* **37,** 2764 (1962).
33. Matsuura, H., Miyazawa, T., and Machida, K., *Spectrochimica Acta* **29A,** 771 (1973).
34. Dluhy, R. A., Mendelsohn, R., Casal, H. L., and Mantsch, H. H., *Biochemistry* **22,** 1170 (1983).
35. Cevc, G., and Marsh, D., *in* ''Phospholipid Bilayers,'' Cell Biology: A Series of Monographs, Vol. 5 p. 17. Wiley, New York, 1987.
36. Casal, H. L., and Mantsch, H. H., *BBA* **779,** 381 (1984).
37. Mantsch, H. H., and McElhaney, R. N., *Chem. Phys. Lipids* **59,** 213 (1991).
38. Kodati, V. R., and Lafleur, M., *Biophys. J.* **64,** 163 (1993).
39. Kodati, R., El-Jastimi, R., and Lafleur, M., *J. Phys. Chem.* **98,** 12191 (1994).
40. Nilsson, A., Holmgren, A., and Lindblom, G. *Biochem.* **30,** 2126 (1991).
41. Blume, A., Hubner, H., Muller, M., and Bauerle, H. D., *Ber. Bunsenges. Phys. Chem.* **92,** 964 (1988).
42. Lewis, R. N. A. H., McElhaney, R. N., Pohle, W., and Mantsch, H. H., *Biophys. J.* **67,** (1994).
43. Heerklotz, H., Binder, H., Lantzsch, G., and Klose, G., *J.Phys. Chem. B* **101,** 639 (1997).
44. Fringeli, U. P., and Gunthard, H. H., *in* ''Molecular Biology, Biochemistry and Biophysics'' (E. Grell, Ed.), p. 270. Springer–Verlag, Berlin/ New York, 1981.
45. Grdadolnik, J., Kidric, J., and Hadzi, D., *Chem. Phys. Lipids* **59,** 57 (1991).
46. Arrondo, J. L. R., Goni, F. M., and Macarulla, J. M., *BBA* **794,** 165 (1984).
47. Matsuura, H., and Fukuhara, K., *J. Phys. Chem.* **91,** 6139 (1987).
48. Matsuura, H., Fukuhara, K., Masatoki, S., and Sakakibara, M., *J. Am. Chem. Soc.* **113,** 1193 (1991).
49. Nilsson, A., Holmgren, A., and Lindblom, G., *Chem. Phys. Lipids* **71,** 119 (1994).
50. Nilsson, P. G., Wennerström, H., and Lindman, B., *J. Phys. Chem.* **87,** 1377 (1983).
51. Luzatti, V., and Tardieu, A., *Annu. Rev. Phys. Chem.* **25,** 79 (1974).
52. Mädler, B., Rapp, G., and Klose, G., in preparation.
53. Ribeiro, A. A., and Dennis, E. A., *Chem. Phys. Lipids* **12,** 31 (1974).

54. Lichtenberg, D., Yedgar, S., Cooper, G., and Gatt, S., *Biochemistry* **18,** 2572 (1979).
55. Israelachvili, J. N., ''Intermolecular and Surface Forces,'' 2nd ed. Academic Press, London, 1991.
56. Andelman, D., Kozlov, M. M., and Helfrich, W., *Europhys. Lett.,* **25,** No. 3, 231 (1994).
57. Thurmond, R. L., Otten, D., Brown, M. F., and Beyer, K., *J. Phys. Chem.* **98,** 972 (1994).
58. Kjellander, R., *J. Chem. Soc. Faraday Trans 2* **78,** 2025 (1982).
59. Kjellander, R., and Florin, E., *J. Chem. Soc. Faraday Trans* **77,** No. 1, 2053 (1981).
60. Andersson, B., and Olofson, G., *Colloid Polym. Sci.* **265,** 318 (1987).
61. Lewis, R. N. A. H., Pohle, W., and McElhaney, R. N., *Biophys. J.* **70,** 2736 (1996).
62. Gill, S. J., and Wadsö, I., *Proc. Natl. Acad. Sci. USA* **73,** 2955 (1976).
63. Wrigley, A. N., Stirton, A. J., and Horward, E. J., *Org. Chem.*, **25,** 4391 (1960).
64. Schnabel, R. J., *J. Labelled Compd. Radiopharm.* **31,** 91 (1992).